Visual Recognition and Detection of Clindamycin by Au@Ag Core–Shell Nanoparticles

Qiuzheng Du,[§] Ziwei Jing,[§] Hang Qi, Lihua Zuo, Lin Zhou, Hua He,* and Zhi Sun*

ACCESS | Metrics & More | Article Recommendations

ABSTRACT: The work described a new colorimetric sensor for the quantitative detection of clindamycin based on Au@Ag core–shell nanoparticles (Au@Ag NPs). The obtained Au@Ag NPs were characterized by transmission electron microscopy (TEM) and ultraviolet and visible spectrophotometry (UV–vis). When Au@Ag NPs were added to a clindamycin solution, it can be observed that the color immediately changed from bright yellow to gray-blue and the absorption spectrum also changed, realizing the visual detection of clindamycin. Under optimal conditions, the absorption ratio (A_{546}/A_{400}) of the UV–vis spectra increased linearly with the concentration of clindamycin ranging from 6.25×10^{-7} to 7.50×10^{-6} mol/L ($R^2 = 0.9945$), with a limit of detection (LOD) of 2.00×10^{-7} mol/L and good recovery of 100.0–102.0% (relative standard deviation (RSD) < 2%). The detection process was convenient without complicated instruments. Compared with other analytes, the Au@Ag NPs detection system has good selectivity for clindamycin. In addition, the Au@Ag NPs colorimetric sensor was successfully used to determine clindamycin in human urine samples. This study provides a simple, rapid, intuitive, and low-cost visualization analysis method of clindamycin, which was helpful for the visualization detection of other targets.
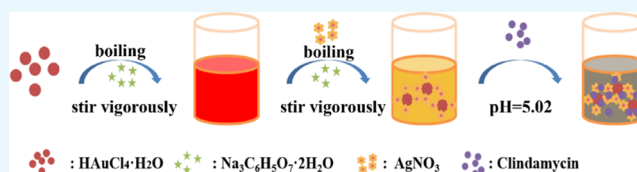
INTRODUCTION

Clindamycin,[1–4] as a lincosamide antibiotic, has a similar mechanism to that of action macrolides. It has a strong inhibitory effect on Gram-positive and Gram-negative anaerobic pathogens, Gram-positive aerobes, and Staphylococcus aureus. However, it often causes local reactions, gastrointestinal reactions, allergic reactions, secondary infections, etc. in clinical use. So the dosage should be accurately monitored to ensure reasonable safety of the medication.

Currently, the detection methods of clindamycin mainly include chemiluminescence,[5] high-performance liquid chromatography-mass spectrometry (HPLC-MS),[6] high-performance liquid chromatography (HPLC),[7] gas–liquid chromatography method (GLC),[8] capillary electrophoresis (CE),[9] microbiological analysis method,[10] adsorption voltammetry,[11] and so on. Although all of the abovementioned methods can be used for the determination of clindamycin, unfortunately, there are also some shortcomings. For example, the operation of GLC is complicated, the CE method has a small injection volume and low sensitivity, the microbiological analysis method has a long cycle and tedious steps, and the electrochemiluminescence (ECL) method has relatively low reproducibility, the possibility of cross-contamination, and environmental sensitivity. According to the structure of clindamycin, it only has weak UV absorption in the low-wavelength range, which is not suitable for the conventional UV method and the fluorescence method. Therefore, it is necessary to develop a more simple, efficient, fast, low-cost, and selective method for the detection of clindamycin.

Recently, the surface plasmon resonance absorption (SPR effect) of noble metallic nanoparticles (such as Au and Ag) has been a hot research direction for the study of trace drug detection with a great potential research value.[12] In particular, silver nanoparticles (Ag NPs), gold nanoparticles (Au NPs), and bimetallic silver/gold nanostructure-based spectral sensors have attracted wide attention in the field of rapid and sensitive analysis.[13–18] Among noble metallic nanoparticles, Au NPs have good stability and biocompatibility, while Ag NPs have more sensitive SPR characteristics and better conductivity. At the same time, Au and Ag have the same lattice constant so they are easy to mix. Compared with a single kind of noble metallic nanoparticles, Au@Ag NPs[19] have not only the advantages of single-metal nanoparticles but also the highly symmetrical dipole resonance and the synergistic effect between bimetallic particles, which can better reflect the SPR effect. In addition, Au@Ag NPs have new optical properties, good stability, and easy size control. At present, Au@Ag NPs have been widely used in biological imaging and biosensing, drug loading, catalysis, and other aspects.[20–22] In addition, the colorimetric sensor based on Au@Ag NPs has realized the

Scheme 1. Preparation of Au@Ag NPs and the Schematic Diagram of Clindamycin Detection

: HAuCl4·H2O   : Na3C6H5O7·2H2O   : AgNO3   : Clindamycin
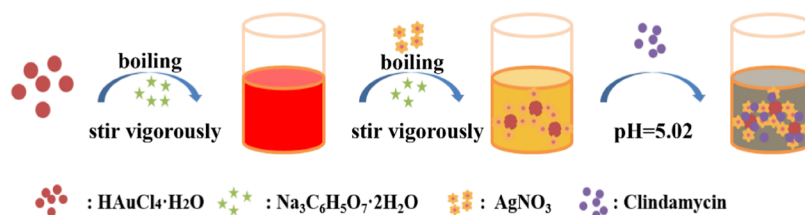
determination of heavy metal ions,[23−25] nuclease,[26] glucose,[27] amino acid,[28] small molecules,[29] and other substances. For example, Zeng et al.[30] prepared Au@Ag NPs with the Au NP-assisted Tollens reaction and used them as a platform to realize the colorimetric sensing of cyanide with a detection limit of 0.4 mM. Sasikumar et al.[31] reported a Au@Ag NP probe for rapid detection of trace cysteamine (CSH) with a detection limit as low as 0.33 nM. In addition, Zhang's group[32] first developed a colorimetric sensor array for detection of oxidizing anions using two core−shell Au@Ag nanoparticles, and it was successfully applied to the recognition of oxidizing anions in river water and tap water samples. However, as far as we know, there are few colorimetric studies on the detection of clindamycin with Au@Ag NPs. The colorimetric method is focused on the recognition of the existence of the target by the naked eye as the color change of the nanoparticle system, which has the characteristics of low cost, fast detection, simple operation, and does not need complex and expensive instruments.[33]

Herein, we have prepared Au@Ag NPs modified by sodium citrate and realized the simple, rapid, and highly sensitive colorimetric sensing to clindamycin using its adjustable SPR characteristics, as shown in Scheme 1. In the presence of clindamycin, Au@Ag NPs aggregated under the action of electrostatic attractive force and hydrogen bond attraction, which made the solution color change from bright yellow to gray-blue and showed a new absorption spectrum. For us, this is the first time to use colorimetry to detect clindamycin in a simple, rapid, and visual way, without large and expensive instruments. In addition, the method has been successfully used for the determination of clindamycin in human urine, which provides a basis for the analysis and detection of trace substances in a clinical complex system. It also provides a new idea for the determination of a weak UV absorption target without a conjugated group.

■ RESULTS AND DISCUSSION

Mechanism of Clindamycin. The surfaces of Au@Ag NPs modified by $Na_3C_6H_5O_7·2H_2O$ are electronegatively charged. They can be uniformly dispersed and stabilized in water through electrostatic repulsion to increase the surface affinity, which is beneficial to the reaction between the substance to be tested and the Au@Ag NPs. From Figure 1A, the stable Au@Ag NPs showed a peak of an SPR absorption band at 400 nm. The methylthio group ($-SCH_3$) on the surface of clindamycin (Figure 2) could form the structure of clindamycin-Au@Ag NPs.[34] The protonation of a tertiary amino group ($-N<$), a primary amino group ($-NH-$), and an ether group ($-O-$) into ($-NH_2^+-$), ($-NH_3^+$), and ($-OH$) structures was beneficial to clindamycin adsorption on Au@Ag NPs by electrostatic interaction. It can be seen that when clindamycin was added, the distribution state, the surface charge density, and the particle size (aggregation) of Au@Ag
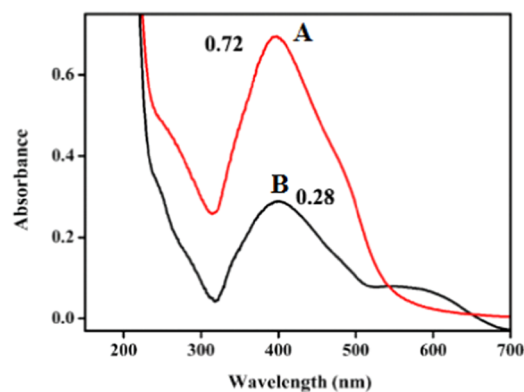
Figure 1. UV−vis absorption spectra of Au@Ag NPs without (A) and with clindamycin ($8 × 10^{-7}$ M) (B).
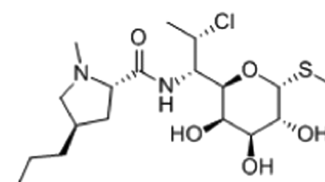
Figure 2. Structure of clindamycin.

NPs changed, resulting in the change of the color of the Au@Ag NP solution (from bright yellow to gray-blue), the absorption peak intensity (decreased at 400 nm), and the absorption wavelength (new absorption band at 546 nm) (Figure 1B). This clustering phenomenon could also be clearly observed in transmission electron microscopy (TEM) images (Figure 3C). Therefore, the change of color and the absorption spectrum of the Au@Ag NPs solution could be developed into a reliable, simple, and rapid UV−vis spectrum or a visual detection method for clindamycin.

Characterization of Au@Ag NPs. The microstructure of Au@Ag NPs was clearly shown by TEM. It can be seen from Figure 3A,B that most of Au@Ag NPs were spherical shaped, homogeneous, evenly distributed, and showed electronic inheterogeneity. In addition, it can be seen from the figure that the dark core of the composite is wrapped by the lighter shell. The inset of Figure 3A exhibits the EDX spectroscopic spectrum of Au@Ag NPs, which can be seen as the presence of gold and silver elements, which are, respectively, located in the middle and outside. Therefore, the preparation of the Au@Ag NPs structure was successful. From the TEM image of Au@Ag NPs, it can be seen that the average particle size of Au@Ag NPs was about 16.7 ± 3.2 nm. Its ζ-potential measurement result was −42.9 ± 1.2 mV (see Figure 4A), which was consistent with the results reported by Zeng et al.[30] The abovementioned results indicated that the surface of the Au@Ag NPs may also be closed by sodium citrate, which increases
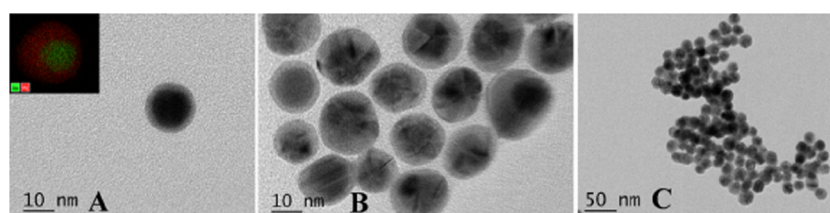
Figure 3. TEM images of Au@Ag NPs before (A and B) and after (C) clindamycin addition; the inset in (A) represents the energy-dispersive X-ray (EDX) elemental map of Au@Ag NPs (the green represents Au and the red represents Ag).
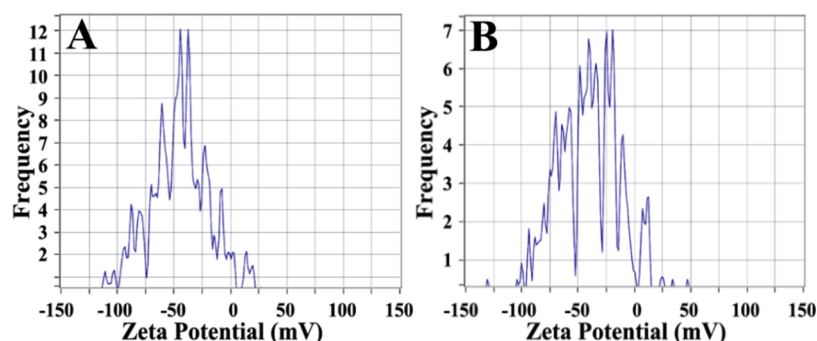
Figure 4. ζ-Potential of Au@Ag NPs before (A) and after (B) clindamycin addition.
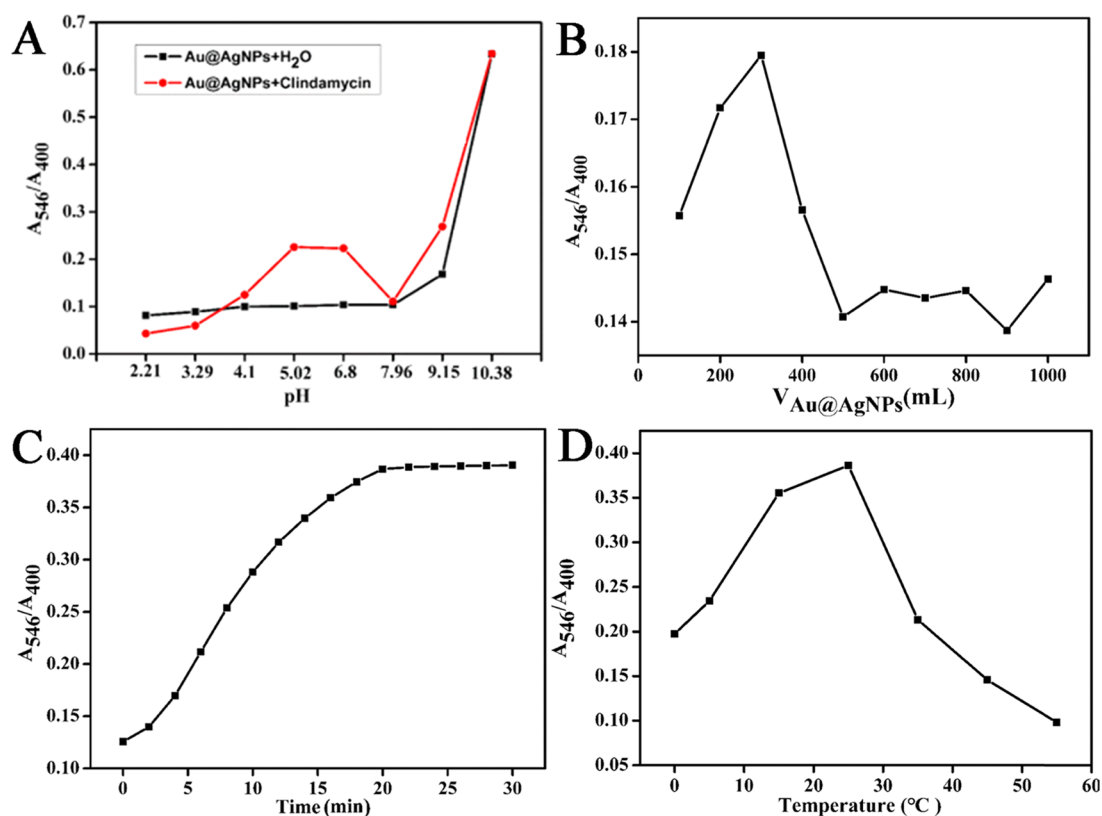
Figure 5. Effect of the pH value (A), Au@Ag NPs concentration (B), incubation time (C), and reaction temperature (D) on the ratio of the A_{546}/A_{400} system.

its stability to make it not aggregated because of electrostatic rejection. Figure 3C shows the characteristics of Au@Ag NPs after adding clindamycin, which has significant aggregation and larger particle size. When clindamycin was added, Au@Ag NPs had obvious aggregation and larger particle size (see Figure 3C), and the ζ-potential also changed (for 39.3 ± 1.1 mV, see Figure 4B).

Optimization of Colorimetric Detection Conditions. To obtain better detection performance and colorimetric conditions, this paper optimized the parameters that affect analysis performance, including the key factors such as the pH value of the solution, Au@Ag NPs concentration, incubation time, and reaction temperature. In this paper, the absorbance ratio at 546 and 400 nm (A_{546}/A_{400}) was selected to evaluate

the aggregation degree of Au@Ag NPs. The higher the ratio, the greater the aggregation degree.

Effect of the pH Value. The existence of Au@Ag NPs is different when the pH of the solution is different. Therefore, the effect of pH on Au@Ag NPs in A_{546}/A_{400} was studied. A BR buffer solution was used to prepare the solution with pH in the range of 2.21–10.38, i.e., pH was 2.21, 3.29, 4.1, 5.02, 6.8, 7.96, 9.15, and 10.38, respectively. Figure 5A (the black line) shows the change of Au@Ag NPs at A_{546}/A_{400} without clindamycin in the pH range of 2.21–10.38. It was found that the Au@Ag NPs were not stable when the pH was 9.15 and 10.38, so they needed to be removed. When the pH < 8, the color of the Au@Ag NP mixed solution remained unchanged, indicating that it was stable. After adding clindamycin (0.2 mL, 3.00×10^{-6} mol/L) (Figure 5A, the red line), the A_{546}/A_{400} ratio increased significantly with the increase of the pH value from 2.21 to 5.02. But when pH < 4 or pH > 7, the absorption ratio (A_{546}/A_{400}) was very low (excluding the two sets of data after deterioration), which was not conducive to the detection of clindamycin. This was due to the fact that the surface of the Au@Ag NPs modified by $Na_3C_6H_5O_7 \cdot 2H_2O$ was filled with ionized citrate anions, which can stably exist without aggregation under the effect of electrostatic repulsion. Because the strong acid environment inhibited the ionization of a citric acid carboxyl group, it could not be protonated. The electrostatic repulsion between Au@Ag NPs was reduced, and the Au@Ag NPs were induced to aggregate. A strong alkali environment had the same mechanism as strong acid. When pH = 5.02, A_{546}/A_{400} reached the maximum value, and a part of the carboxyl group of citric acid dissociated into an anion with a negative charge. However, the other part did not dissociate. The protonated clindamycin has a positive charge. At this time, the electrostatic attraction was the largest. Under the action of hydrogen bonding interaction and electrostatic attraction, the surface charges of the Au@Ag NPs were reduced, resulting in agglomeration. Therefore, the pH value of 5.02 was selected for further optimization.

Effect of Au@Ag NP Concentration. The concentration of Au@Ag NPs has a great influence on the interaction between Au@Ag NPs and clindamycin. Therefore, the change in system absorbance caused by Au@Ag NPs in the volume range of 0.10–1.00 mL was investigated. In Figure 5B, when Au@Ag NPs were added in a lower amount, the sensitivity of the system reaction was higher, and the aggregation was more likely to occur. It was because nanoparticles with low concentration are more likely to have electrostatic interaction with the drug in the same volume. As the concentration of Au@Ag NPs increased, the amount of clindamycin was gradually insufficient to react with it. The absorption ratio (A_{546}/A_{400}) was lower than that of low concentrations, so the sensitivity was significantly reduced. After the volume of Au@Ag NPs was increased to more than 0.40 mL, the absorbance ratio (A_{546}/A_{400}) rapidly decreased to a very low level, no obvious visualization phenomenon could be observed, and accurate quantitative analysis could not be carried out. Therefore, a high concentration of Au@Ag NPs was not suitable for practical applications. When the volume of Au@Ag NPs was increased up to 0.30 mL, the absorption ratio (A_{546}/A_{400}) reached the maximum and the reaction was most obvious. However, a too rapid and violent reaction at a lower concentration leads to errors and the experimental operation becomes difficult. Therefore, a moderate concentration of 0.40 mL was used. At this concentration, the reaction was easy to

control and the light absorption ratio (A_{546}/A_{400}) was more appropriate

Effect of Incubation Time. The incubation time of Au@Ag NPs and clindamycin was an important factor affecting the aggregation of Au@Ag NPs. From Figure 5C, it can be seen that the absorption ratio (A_{546}/A_{400}) increased rapidly in the initial 20 min of the reaction. The absorption ratio (A_{546}/A_{400}) increased slowly and remained almost unchanged after the incubation time exceeded 20 min, indicating that the aggregation reaction was basically completed at 20 min. Therefore, the incubation time of 20 min was chosen for UV detection.

Effect of Reaction Temperature. The reaction temperature has a great influence on the interaction between Au@Ag NPs and clindamycin. As shown in Figure 5D, the absorption ratio (A_{546}/A_{400}) was the highest at 25 °C. When the temperature was higher than 25 °C, the molecular motion was severe, which restrained the interaction between the molecules. When the temperature was below 25 °C, the reaction rate was slower. Therefore, room temperature (25 °C) was chosen for experiments.

Selectivity Investigation of the Au@Ag NP Detection System. To investigate the practicability of this method, the selectivity of this method was investigated. Urine composition mainly refers to water, glucose, protein, inorganic salts, and some small molecular particles. Therefore, the coexisting substances such as sugars (glucose and lactose), amino acids (threonine and serine), and potential interfering ions (Na^+, K^+, Ca^{2+}, NH_4^+, Cl^-, SO_4^{2-}, and PO_4^{3-}) were detected. Clindamycin (5.00×10^{-6} mol/L) and other analytes (5.00×10^{-4} mol/L) were added to the Au@Ag NP solution to obtain each mixed solution. Figure 6 shows the ratio A_{546}/A_{400}
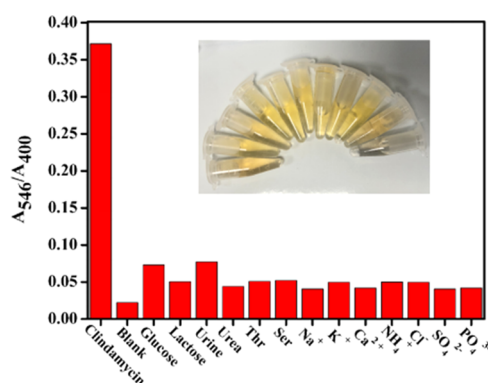
Figure 6. Visualized color change and the absorption ratio A_{546}/A_{400} of Au@Ag NP solutions in the presence of clindamycin (5.00×10^{-6} mol/L) and other analytes (5.00×10^{-4} mol/L). The experiments were performed at pH = 5.02, $V_{Au@Ag\ NPs}$ of 0.4 mL, incubation time of 20 min, and room temperature.

of Au@Ag NPs, and the visual color changed under each coexisting substance. When clindamycin was added to the Au@Ag NP micelle solution, the ratio of A_{546}/A_{400} was higher and there was a significant color change (see illustration); while, when other interfering substances were added to the Au@Ag NP micelle solution, the ratio of A_{546}/A_{400} was almost unchanged, and there was no visible color change. Therefore, the abovementioned data could prove that this method had good selectivity for the detection of clindamycin, and 100 times of coexisting substances had little effect on Au@Ag NPs.
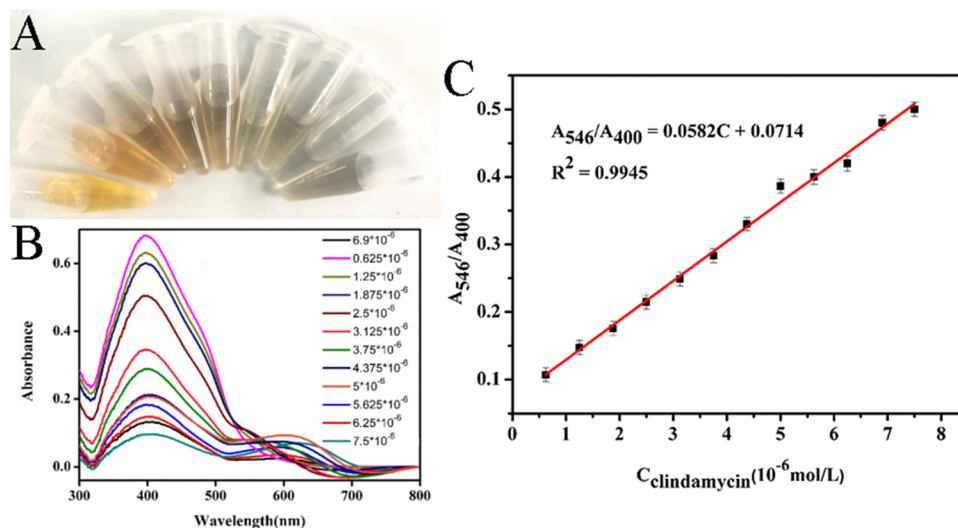
Figure 7. (A) Image of Au@Ag NPs when clindamycin concentration increased from 6.25×10^{-7} to 7.50×10^{-6} mol/L, (B) UV−vis absorption spectra of Au@Ag NPs in the presence of clindamycin at different concentrations, and (C) standard curve of the absorption ratio (A_{546}/A_{400}) versus the concentration of clindamycin in the range of 6.25×10^{-7}−7.50×10^{-6} mol/L. Experimental conditions: pH = 5.02, $V_{Au@Ag\ NPs}$ of 0.4 mL, incubation time of 20 min, and room temperature.

This detection system had a strong anti-interference ability, which could be used to detect trace clindamycin in urine.

Quantitative Detection of Clindamycin. The best reaction condition was confirmed after optimized experiments. Under this condition, the concentration of clindamycin was measured and the probe colorimetry and the standard working curve were established. The clindamycin solution with a concentration range of 3.25×10^{-7}−9.00×10^{-6} mol/L was added to the Au@Ag NPs solution. As shown in Figure 7A, as the concentration of clindamycin increased, the Au@Ag NPs reaction system had obvious visualization phenomena, which were bright yellow, orange, yellow-brown, and blue-gray, in turn. Therefore, the method of color recognition to determine the concentration of clindamycin was simple, rapid, and did not need precise instruments. In addition, UV−vis absorption spectrometry was used to detect the concentrations of clindamycin, and the results are shown in Figure 7B. It can be seen that as the concentration increased, the plasmon resonance absorption peak at 400 nm gradually decreased. A new and gradually increasing absorption peak appeared at 546 nm, and the wavelength was gradually red-shifted. That is probably because with the reaction between the outer Ag NPs and clindamycin, the inner Au NPs gradually exposed and gathered, and the absorption peak of Au NPs appeared. The size of the gold nanoparticle increased due to the aggregation, and the absorption peak was red-shifted. As shown in Figure 7C, the absorption ratio (A_{546}/A_{400}) of the reaction system has a benign linear relationship within the range of 6.25×10^{-7}−7.5×10^{-6} mol/L clindamycin concentration. The standard regression equation was as follows: A_{546}/A_{400} = 0.0582C + 0.0714, R^2 = 0.9945, and the limit of detection (LOD) was 2.00×10^{-7} mol/L (3S/N).

The repeatability of Au@Ag NPs was investigated. Six glass test tubes were taken in which a 5.00×10^{-6} mol/L clindamycin solution was added to the Au@Ag NP solution; they were allowed to stand for 20 min. The system absorption ratio A_{546}/A_{400} was measured in parallel and the relative standard deviation (RSD) value was calculated. The experimental results are shown in Table 1. The RSD value

Table 1. Repeatability of the Clindamycin Determination Method

sample	A_{546}/A_{400}	C ($\times 10^{-6}$ mol/L)	$C_{average}$ ($\times 10^{-6}$ mol/L)	RSD (%)
1	0.363	5.009		
2	0.360	4.961		
3	0.368	5.104	5.04	1.57
4	0.365	5.044		
5	0.372	5.156		
6	0.360	4.958		

was equal to 1.57%, indicating that the repeatability of the method meets the requirements. In addition, 3.00×10^{-6}, 5.00×10^{-6}, and 7.00×10^{-6} mol/L clindamycin solutions were prepared, respectively, with each concentration of three parts. Then, the UV spectrum of the clindamycin reaction system was measured according to the standard curve determination method, and the recovery rate was calculated as 100.0−102.0% and the RSD value was <2%, indicating that the accuracy of this method was good.

As shown in Table 2, compared with the reported methods for detecting clindamycin, this method has a lower LOD and

Table 2. Comparison of Different Methods Reported for Clindamycin Detection

analysis method	sample matrix	concentration range (μg/mL)	LOD (ng/mL)	refs
HPLC	skin	0.50−20.0	120	7
HPLC/UV	serum	0.08−6.0	60	35
CE	urine	0.21−42.5	5.52	9
CE-ECL	urine	0.21−42.5	59.50	36
UV	urine	0.27−3.19	85.00	this method

higher sensitivity. In addition, this method also has the advantages of simple operation, short time consumption, low requirements for instruments, and visualization of results.

Detection of Clindamycin in Human Urine Samples. Au@Ag NPs were added to the diluted urine samples containing clindamycin with different concentrations in the

range from 6.00×10^{-7} to 8.00×10^{-6} mol/L. The results are shown in Figure 8; with the increase in the concentration of
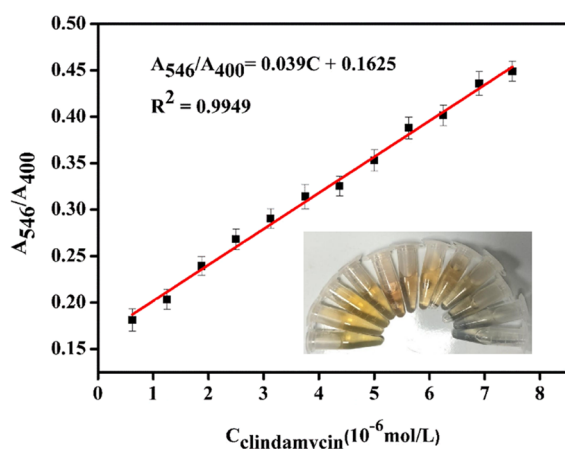
Figure 8. Absorption ratio (A_{546}/A_{400}) and the color change chart with the concentration of clindamycin in the urine sample of $9.00 \times 10^{-7}-7.50 \times 10^{-6}$ mol/L.

clindamycin in the urine samples, the color gradually changed. The color of clindamycin in the linear experiment could be compared with the naked eye, so the concentration of clindamycin in the urine samples could be directly judged without using large-scale instruments. The absorption ratio (A_{546}/A_{400}) of the Au@Ag NPs reaction system has a benign linear relationship in the range of clindamycin concentration of $9.00 \times 10^{-7}-7.50 \times 10^{-6}$ (see Figure 8). The standard regression equation was as follows: $A_{546}/A_{400} = 0.039C + 0.1625$ ($R^2 = 0.9949$). The LOD and the limit of quantification (LOQ) were 3.00×10^{-7} mol/L (3S/N) and 1.0×10^{-6} mol/L (10S/N), respectively.

The diluted urine was used to prepare three clindamycin solutions with concentrations of 1.50×10^{-6}, 3.50×10^{-6}, and 5.50×10^{-6} mol/L, respectively. Then, the UV spectrum of the clindamycin reaction system was measured according to the standard curve method and the recovery rate was calculated. The results are shown in Table 3; the average recovery range was 99.0−101.0% and the RSD value was <2%, which indicated that the Au@Ag NPs had good and reliable colorimetric detection accuracy for clindamycin in human urine samples.

Table 3. Detection Results of Clindamycin in Urine Samples Using This Method[a]

sample	added amount ($\times 10^{-6}$ mol/L)	found amount ($\times 10^{-6}$ mol/L)	recovery (%)	RSD ($n = 3$, %)
1	1.50	1.50	100.20	0.84
2		1.49		
3		1.52		
1	3.50	3.53	99.13	1.54
2		3.42		
3		3.46		
1	5.50	5.47	100.80	1.11
2		5.55		
3		5.60		

[a]Experimental conditions: pH = 5.02, $V_{Au@Ag NPs}$ of 0.4 mL, incubation time of 20 min, and room temperature.

CONCLUSIONS

In conclusion, a new visual detection method of clindamycin based on SPR characteristics of Au@Ag NPs was established by seed synthesis. The principle of visual detection could be attributed to the fact that under the appropriate pH value (pH = 5.02), clindamycin and Au@Ag NPs could reduce the electrostatic repulsion between Au@Ag NPs through electrostatic attraction and hydrogen bond interaction, thus inducing their aggregation, resulting in the change of the solution color from bright yellow to gray-blue and the red shift of the SPR peak. Compared with other methods, this method was simple, visible, and did not need complex instruments. The detection range of Au@Ag NPs was wide, and the LOD was low (2.00×10^{-7} mol/L). It had a good linear response to clindamycin in the range of $6.25 \times 10^{-7}-7.5 \times 10^{-6}$ mol/L. The LOD and LOQ of clindamycin in urine were 3.00×10^{-7} and 1.0×10^{-6} mol/L, respectively. More importantly, it could be used for rapid detection of samples without complex pretreatment and chemical modification. Therefore, Au@Ag NPs used as the sensor in this study provide not only a simple and efficient method for clindamycin detection but also new prospects for the development of more sensitive clinical detection methods.

EXPERIMENTAL SECTION

Instruments and Reagents. Chloroauric acid (HAuCl₄·4H₂O, >99.9%) was obtained from Shanghai Aladdin Reagent Database Inc. Trisodium citrate dihydrate (Na₃C₆H₅O₇·2H₂O) was supplied by Shanghai Rongrun Chemical Reagent Co. Silver nitrate (AgNO₃) was obtained from Sinopharm Chemical Reagent Co., Ltd. Sodium hydroxide (NaOH, >96%) was obtained from Sinopharm Chemical Reagent Co., Ltd. Clindamycin was supplied by the China National Institute for Food and Drug Control. Acetic acid, phosphoric acid, nitric acid, concentrated hydrochloric acid, and boric acid were purchased from Saen Chemical Technology, Ltd. All reagents were of analytical grade and were used directly without further treatment. Deionized water was used throughout the experiment.

The obtained samples were characterized by transmission electron microscopy (TEM, FEI Tecnai G2 F20). Energy-dispersive X-ray (EDX) elemental mapping measurements were collected using an X-max 80 T (Oxford, U.K.). The ζ value was measured using a Zetasizer Nano ZS90 (Malvern Instruments, U.K.). UV−vis absorption spectra were recorded on a UV−vis spectrophotometer (UV-1800, Shimadzu, Japan) at room temperature. The heating test was carried out on a magnetic heating agitator (79-1, Jiangsu Guohua instrument factory, China). All pH values were measured using a pH meter (pHS-25, Shanghai Weiye Instrument Factory, China).

Preparation of Sodium Citrate-Stabilized Au@Ag NPs. All glassware were thoroughly cleaned with newly prepared aqua regia (1:3 HNO₃/HCl), then cleaned with Milli-Q water, and finally placed in an oven until completely dry before use. The preparation of Au@Ag NPs was based on the synthesis of seed gold nanoparticles and the reduction of AgNO₃ on its surface. In short, 1% Na₃C₆H₅O₇·2H₂O (1.25 mL, 3.88×10^{-2} mol/L) was rapidly added to the heated and boiling HAuCl₄·4H₂O (50 mL, 2.94×10^{-4} mol/L) and stirred vigorously for 20 min to obtain a red liquid. Then, AgNO₃ (3 mL, 5.88×10^{-3} mol/L) and Na₃C₆H₅O₇·2H₂O (0.75 mL, 3.88×10^{-2} mol/L) were added slowly and stirred vigorously for 60 min in a boiling state, and then cooled naturally to room

temperature to obtain brownish-yellow Au@Ag NPs, which were preserved at 4 °C for standby.

Colorimetric Detection of Clindamycin. Usually, 5 mL test tubes were added with a Au@Ag NPs solution (0.40 mL), a Britton−Robinson (BR) buffer solution (0.20 mL, pH 5.02), and a clindamycin solution (0.20 mL) with different concentrations. After incubating at room temperature for 20 min, the UV−vis absorption spectra were recorded using a UV−vis spectrophotometer in the range of 300−800 nm, and the color of the Au@Ag NPs solution was recorded with a camera. The experiment used the ratio of the UV−vis absorption spectrum (A_{546}/A_{400}) at 546 and 400 nm to quantify the concentration of clindamycin.

Determination of Clindamycin in Human Urine Samples. Urine samples were collected from healthy volunteers. All samples were diluted 200-fold with Milli-Q water before use, and then a series of urine samples containing different concentrations of clindamycin were prepared. After incubation for 20 min, the UV−vis absorption spectra of Au@Ag NPs in A_{546}/A_{400} were recorded.

■ AUTHOR INFORMATION

Corresponding Authors

Hua He − *Department of Analytical Chemistry, China Pharmaceutical University, Nanjing, Jiangsu 211100, China*; Phone: +86 025 86185160; Email: dochehua@163.com

Zhi Sun − *Department of Pharmacy, The First Affiliated Hospital of Zhengzhou University, Zhengzhou 450052, China*; orcid.org/0000-0001-6007-4923; Phone: +86 025 66862570; Email: sunzhi2013@163.com

Authors

Qiuzheng Du − *Department of Pharmacy, The First Affiliated Hospital of Zhengzhou University, Zhengzhou 450052, China*

Ziwei Jing − *Department of Pharmacy, The First Affiliated Hospital of Zhengzhou University, Zhengzhou 450052, China*

Hang Qi − *Department of Analytical Chemistry, China Pharmaceutical University, Nanjing, Jiangsu 211100, China*

Lihua Zuo − *Department of Pharmacy, The First Affiliated Hospital of Zhengzhou University, Zhengzhou 450052, China*

Lin Zhou − *Department of Pharmacy, The First Affiliated Hospital of Zhengzhou University, Zhengzhou 450052, China*

Complete contact information is available at:
https://pubs.acs.org/10.1021/acsomega.1c01028

Author Contributions

§Q.D. and Z.J. contributed equally to this work and should be considered co-first authors.

Notes

The authors declare no competing financial interest.

■ REFERENCES

(1) Morar, M.; Bhullar, K.; Hughes, D. W.; Junop, M.; Wright, G. D. Structure and mechanism of the lincosamide antibiotic adenylyltransferase LinB. *Structure* **2009**, *17*, 1649−1659.

(2) Batzias, G. C.; Delis, G. A.; Athanasiou, L. V. Clindamycin bioavailability and pharmacokinetics following oral administration of clindamycin hydrochloride capsules in dogs. *Vet. J.* **2005**, *170*, 339−345.

(3) He, J.; Wu, N.; Luo, P.; Guo, P.; Qu, J.; Zhang, S.; Zou, X.; Wu, F.; Xie, H.; Wang, C.; Jiang, W. Development of a heterologous enzyme-linked immunosorbent assay for the detection of clindamycin and lincomycin residues in edible animal tissues. *Meat Sci.* **2017**, *125*, 137−142.

(4) Cho, S. H.; Im, H. T.; Park, W. S.; Ha, Y. H.; Choi, Y. W.; Lee, K. T. Simple method for the assay of clindamycin in human plasma by reversed-phase high-performance liquid chromatography with UV detector. *Biomed. Chromatogr.* **2005**, *19*, 783−787.

(5) Shao, X.; Xie, X.; Liu, Y.; Song, Z. Rapid determination of clindamycin in medicine with myoglobin-luminol chemiluminescence system. *J. Pharm. Biomed. Anal.* **2006**, *41*, 667−670.

(6) Girondi, N. G.; Barreto, F.; Pigatto, M. C.; Dalla Costa, T. Sensitive analytical method to quantify clindamycin in plasma and microdialysate samples: Application in a preclinical pharmacokinetic study. *J. Pharm. Biomed. Anal.* **2018**, *153*, 57−62.

(7) Pereira, M. N.; Matos, B. N.; Gratieri, T.; Cunha-Filho, M.; Gelfuso, G. M. Development and validation of a simple chromatographic method for simultaneous determination of clindamycin phosphate and rifampicin in skin permeation studies. *J. Pharm. Biomed. Anal.* **2018**, *159*, 331−340.

(8) Brown, L. W. GLC determination of clindamycin and related compounds. *J. Pharm. Sci.* **1974**, *63*, 1597−1600.

(9) Liu, Y. M.; Shi, Y. M.; Liu, Z. L.; Peng, L. F. Sensitive determination of tilmicosin, erythromycin ethylsuccinate and clindamycin by CE with electrochemiluminescence detection using azithromycin as internal standard and its applications. *J. Sep. Sci.* **2010**, *33*, 1305−1311.

(10) Sobottka, I.; Wegscheider, K.; Balzer, L.; Boger, R. H.; Hallier, O.; Giersdorf, I.; Streichert, T.; Haddad, M.; Platzer, U.; Cachovan, G. Microbiological analysis of a prospective, randomized, double-blind trial comparing moxifloxacin and clindamycin in the treatment of odontogenic infiltrates and abscesses. *Antimicrob. Agents Chemother.* **2012**, *56*, 2565−2569.

(11) Habib, I. H. I.; Rizk, M. S.; El-Aryan, T. R. Determination of clindamycin in dosage forms and biological samples by adsorption stripping voltammetry with carbon paste electrode. *Pharm. Chem. J.* **2011**, *44*, 705−710.

(12) Bharath, G.; Prakash, J.; Rambabu, K.; Venkatasubbu, G. D.; Kumar, A.; Lee, S.; Theerthagiri, J.; Choi, M. Y.; Banat, F. Synthesis of TiO2/RGO with plasmonic Ag nanoparticles for highly efficient photoelectrocatalytic reduction of CO2 to methanol toward the removal of an organic pollutant from the atmosphere. *Environ. Pollut.* **2021**, *281*, No. 116990.

(13) Xie, X.; Pu, H.; Sun, D. W. Recent advances in nanofabrication techniques for SERS substrates and their applications in food safety analysis. *Crit. Rev. Food Sci. Nutr.* **2018**, *58*, 2800−2813.

(14) Guo, Z.; Jia, Y.; Song, X.; Lu, J.; Lu, X.; Liu, B.; Han, J.; Huang, Y.; Zhang, J.; Chen, T. Giant Gold Nanowire Vesicle-Based Colorimetric and SERS Dual-Mode Immunosensor for Ultrasensitive Detection of Vibrio parahemolyticus. *Anal. Chem.* **2018**, *90*, 6124−6130.

(15) Ye, H.; Yang, K.; Tao, J.; Liu, Y.; Zhang, Q.; Habibi, S.; Nie, Z.; Xia, X. An Enzyme-Free Signal Amplification Technique for Ultrasensitive Colorimetric Assay of Disease Biomarkers. *ACS Nano* **2017**, *11*, 2052−2059.

(16) Wang, K.; Sun, D. W.; Pu, H.; Wei, Q. Shell thickness-dependent Au@Ag nanoparticles aggregates for high-performance SERS applications. *Talanta* **2019**, *195*, 506−515.

(17) Lee, Y. J.; Park, Y. Green Synthetic Nanoarchitectonics of Gold and Silver Nanoparticles Prepared Using Quercetin and Their

Cytotoxicity and Catalytic Applications. *J. Nanosci. Nanotechnol.* **2020**, *20*, 2781−2790.

(18) Lee, S. H.; Jung, H. J.; Lee, S. J.; Theerthagiri, J.; Kim, T. H.; Choi, M. Y. Selective synthesis of Au and graphitic carbon-encapsulated Au (Au@GC) nanoparticles by pulsed laser ablation in solvents: Catalytic Au and acid-resistant Au@GC nanoparticles. *Appl. Surf. Sci.* **2020**, *506*, No. 145006.

(19) Samal, A. K.; Polavarapu, L.; Rodal-Cedeira, S.; Liz-Marzan, L. M.; Perez-Juste, J.; Pastoriza-Santos, I. Size tunable Au@Ag core-shell nanoparticles: synthesis and surface-enhanced Raman scattering properties. *Langmuir* **2013**, *29*, 15076−15082.

(20) Luo, Z.; Zheng, K.; Xie, J. Engineering ultrasmall water-soluble gold and silver nanoclusters for biomedical applications. *Chem. Commun.* **2014**, *50*, 5143−5155.

(21) Amoli-Diva, M.; Sadighi-Bonabi, R.; Pourghazi, K.; Hadilou, N. Tunable Surface Plasmon Resonance-Based Remote Actuation of Bimetallic Core-Shell Nanoparticle-Coated Stimuli Responsive Polymer for Switchable Chemo-Photothermal Synergistic Cancer Therapy. *J. Pharm. Sci.* **2018**, *107*, 2618−2627.

(22) Jiang, H. L.; Akita, T.; Ishida, T.; Haruta, M.; Xu, Q. Synergistic catalysis of Au@Ag core-shell nanoparticles stabilized on metal-organic framework. *J. Am. Chem. Soc.* **2011**, *133*, 1304−1306.

(23) Zhang, J.; Zhu, K.; Hao, H.; Huang, G.; Gan, W.; Wu, K.; Zhang, Z.; Fu, X. A novel chitosan modified Au@Ag core-shell nanoparticles sensor for naked-eye detection of Hg^{2+}. *Mater. Res. Express* **2019**, *6*, No. 125045.

(24) Chen, W. Y.; Lan, G. Y.; Chang, H. T. Use of fluorescent DNA-templated gold/silver nanoclusters for the detection of sulfide ions. *Anal. Chem.* **2011**, *83*, 9450−9455.

(25) Chung, E.; Gao, R.; Ko, J.; Choi, N.; Lim, D. W.; Lee, E. K.; Chang, S. I.; Choo, J. Trace analysis of mercury(II) ions using aptamer-modified Au/Ag core-shell nanoparticles and SERS spectroscopy in a microdroplet channel. *Lab Chip* **2013**, *13*, 260−266.

(26) Yuan, P.; Ma, R.; Gao, N.; Garai, M.; Xu, Q. H. Plasmon coupling-enhanced two-photon photoluminescence of Au@Ag core-shell nanoparticles and applications in the nuclease assay. *Nanoscale* **2015**, *7*, 10233−10239.

(27) Kang, F.; Hou, X.; Xu, K. Highly sensitive colorimetric detection of glucose in a serum based on DNA-embeded Au@Ag core-shell nanoparticles. *Nanotechnology* **2015**, *26*, No. 405707.

(28) Wang, R.; Yu, Z. Validity and Reliability of Benesi-Hildebrand Method. *Acta Phys.-Chim. Sin.* **2007**, *23*, 1353−1359.

(29) Tang, L.; Li, S.; Han, F.; Liu, L.; Xu, L.; Ma, W.; Kuang, H.; Li, A.; Wang, L.; Xu, C. SERS-active Au@Ag nanorod dimers for ultrasensitive dopamine detection. *Biosens. Bioelectron.* **2015**, *71*, 7−12.

(30) Zeng, J. B.; Cao, Y. Y.; Chen, J. J.; Wang, X. D.; Yu, J. F.; Yu, B. B.; Yan, Z. F.; Chen, X. Au@Ag core/shell nanoparticles as colorimetric probes for cyanide sensing. *Nanoscale* **2014**, *6*, 9939−9943.

(31) Sasikumar, T.; Ilanchelian, M. A simple assay for direct visual and colorimetric sensing application of cysteamine using Au@Ag core-shell nanoparticles. *Opt. Mater.* **2020**, *109*, No. 110237.

(32) Zhang, C.; Li, L.; Liu, Q.; Chen, Z. Colorimetric Differentiation of Multiple Oxidizing Anions Based on Two Core-Shell Au@Ag Nanoparticles with Different Morphologies as Array Recognition Elements. *Anal. Chem.* **2020**, *92*, 7123−7129.

(33) Chen, H.; Fang, A.; Zhang, Y.; Yao, S. Silver triangular nanoplates as an high efficiently FRET donor-acceptor of upconversion nanoparticles for ultrasensitive "Turn on-off" protamine and trypsin sensor. *Talanta* **2017**, *174*, 148−155.

(34) Holmes, S.; Palmer, R. E.; Guo, Q. Diffusion of $Au(CH_3S)_2$ on Au(III) Observed with the Scanning Tunneling Microscope. *J. Phys. Chem. C* **2019**, *123*, 24104−24110.

(35) Batzias, G. C.; Delis, G. A.; Koutsoviti-Papadopoulou, M. A new HPLC/UV method for the determination of clindamycin in dog blood serum. *J. Pharm. Biomed. Anal.* **2004**, *35*, 545−554.

(36) Wang, J.; Peng, Z.; Yang, J.; Wang, X.; Yang, N. Detection of clindamycin by capillary electrophoresis with an end-column electrochemiluminescence of tris(2,2'-bypyridine)ruthenium(II). *Talanta* **2008**, *75*, 817−823.